Communications of BAO, Vol. 70, Issue 1, 2023, pp. 23–26

Long period fluctuations of solar active regions

G. Dumbadze*[1,2]

[1]Evgeni Kharadze Georgian National Astrophysical Observatory, M. Kostava street 47/57, 0179 Tbilisi, Georgia
[2]Centre for Computational Helio Studies, Ilia State University, G. Tsereteli str 3, 0162 Tbilisi, Georgia

Abstract

The fluctuation spectra of solar active regions (ARs) contain information about the geometrical features and ground physical processes responsible for the appearance of such a background vibration noise. The investigation is based on an analysis of a time series built photospheric magnetograms and comprises case studies of several types of AR structures. We detect characteristic properties of Fourier and wavelet spectra evaluated for the solar active region area and radial magnetic flux time series. There are long-period oscillations, similarly to the characteristic lifetimes of super-granulation, determined from the datasets of the AR total area and radial magnetic flux, respectively. According to our results the fluctuation spectra of the AR areas and radial magnetic fluxes somewhat differ from each other both in terms of values of the spectral power-law exponents, as well as their variability ranges in different consider cases. The characteristic properties of the area and radial magnetic flux fluctuation spectra for the ARs show noticeable discrepancies between each other. It can also be concluded that behind the formation of AR area and radial flux vibration spectra might be different physical mechanisms in action.

Keywords: *solar active regions; oscillations; data analysis.*

1. Introduction

The active regions (ARs) are the complex magnetic structures that emerging on the solar surface. ARs have many sunspots which number, location, and size vary in time. So, the sunspots can be considered as the indicator of the solar magnetic activity. The ARs show complex morphology and dynamics that determine the different types of waves and oscillatory motions. The study of these oscillations can be divided into some branches: umbral chromospheric oscillations with a typical period of three minutes (Centeno et al., 2006, Chorley et al., 2010); umbral photospheric oscillations with a typical period of five minutes (Shergelashvili & Poedts, 2005, Thomas et al., 1984); long-period oscillations with a typical period of several hours (Dumbadze et al., 2017, Efremov et al., 2007); and ultra-long-period oscillations of sunspot umbrae, with typical periods of several days (Gopasyuk, 2004, Khutsishvili et al., 1998).

The target of the present paper is to find the long-period oscillations in different types of ARs and to more systematically examine the existence of them. For this purpose, we selected the ARs according to their morphological structure and study them along their transit across the solar disk. This paper is organized as follows: the data of the observations of the ARs and the data processing methods are described in Sect. 2. The The analysis and discussion of the discovered significant periods are given in Sect. 3. The conclusions are presented in Sect. 4.

2. Methods

For our investigation, the five ARs are selected according to their morphology types so that the observational time span include from roughly $-70°$ to $+70°$ longitude. The data is taken from the Solar Dynamics Observatory (SDO)/Helioseismic and Magnetic Imager (HMI) (Scherrer et al., 2012). Namely, the line-of-sight magnetogram (B_{LOS}) dataset of 45 s cadence is used for the investigation, where the projection effects are corrected using the azimuthal equidistant (Postel) projection. In addition, there are used three components of the magnetic field (*i.e.*, radial B_r, meridional B_θ, and azimuthal B_φ) dataset of 720 s cadence,

*gdumbadze@abao.ge

which are obtained from Space-weather HMI Active Region Patches (SHARP, Bobra et al. (2014)), where the projection effects are corrected using cylindrical equal-area mapping.

We calculate the active pixels of the original B_{LOS} magnetograms (or B_r, B_θ and B_φ) using the thresholds from the $\pm$ 300 − 400 G range. The value of the threshold is chosen individually for each different ARs, so that the spurious small magnetic features around the AR are filtered out, while the main components of the AR remain visible. Using the sequence of snapshots within the observational time span, we produce the time series of the total unsigned radial magnetic flux, determined as

$$|\Phi| = \sum_{\text{active pixels}} |B_r(x,y)|S(x,y), \tag{1}$$

where $B_r(x,y)$ is the radial magnetic field component in each active pixel, and $S(x,y) = 1.33 \times 10^5$ km^2 is the area covered by these pixels on the solar surface corresponding to the cylindrical equal area remapping (Bobra et al., 2014). In addition, we produce the time series for the total areas of the studied ARs for all components of the magnetic field as the total number of the active pixels.

In order to find the characteristic periods, we use three different methods for the period detection: (i) The first method that we use is suggested by Vaughan, that implies to find significant peaks on top of the power-law noise. Using this method, the periodograms of the detrended and apodised datasets are computed and plotted on log-space. To find the peaks above the confidence level, a linear model fit of the obtained power spectrum are plotted. We assume that computed power has the second order two-dimensional chi-square (χ^2_2) distribution as a null hypothesis. The goodness of the model is checked by Kolmogorov-Smirnov (KS) test (Press et al., 2007). If the KS test does not satisfy the null hypothesis, we adjust the slope and the offset until the test is fulfilled. We estimate the 95% probability limit by assuming that the noise is two-dimensional chi-square distributed using the computed slopes and offset coefficients. All peaks above this line can be assumed as outlying periods and those below this line belong to noise. (ii) The second method we use is a method of the spectral re-binning (Appourchaux, 2003) to increase the significant peaks in the power spectrum. It increases outlying peaks and reduce the noise. As an above, the detrendization and apodization also are applied to the dataset. Then, there are computed periodograms and sum the power of every two consecutive bins and divided sum by two. Everything is repeated as in first method, but in this case, instead of a two-dimensional χ^2_2 distribution function, we use a four-dimensional distribution function χ^2_4. (iii) To reduce the noise, we use the method based on the division of the original dataset. The original dataset is divided into four equivalent non-overlapping intervals of time. Each of these intervals are derived the power spectra and summed. In this case, everything is repeated as in the first method. The peaks found by M1 and M2 can be recognized as 'real', if they still remain in the summed spectrum. The multi-method analysis allows us to confirm the significant periods by different methods.

3. Discussion

The long-period oscillations in ARs are studying using the Fourier spectra of the time series, which have certain observational time spans and sampling rates. The period resolution and accuracy of the obtained power spectra are determined by the characteristic parameters of the datasets. As a result, some significant periods in the spectra are included in a strong background noise that have a power-law nature.

The most populated sets of the periods are revealed for the total area of the ARs, while the radial unsigned magnetic flux data has some significant periods. The most frequently detected periods are about 6- and 4.7-hour. These periods are found in the radial unsigned magnetic flux and the total area oscillations in almost all ARs. The frequent presence of these periods might be linked to the periodic flux emergence or cancellation processes. In all analyzed datasets the long-period peaks that are longer than 10 hours can be detected less frequently than those of shorter periods. The evident reason for this is the gradual growth of spectral uncertainty of the periods. This also is accompanied with the presence of two artificial instrumental peaks at 12- and 24-hour (Liu et al., 2012). These two instrumental peaks can mix the 'real' peaks with artificial spectral ones. Probably, these artificial signals does not have enough impact on the spectrum below 10-hour. In general, we show that in all datasets there are long-period oscillations with characteristic periods in the range from 2 to 20 hours. These periods are similar to the characteristic lifetimes of the super-granulation. So, the observed oscillation periods can be intuitively connected with the characteristic turnover times of the super-granulation cells.

We group together the obtained significant periods as the following ranges: (i) 'harmonic' P_1 – 17.1 $\pm$ 0.71 − 17.4 $\pm$ 0.74 hours (marked in cyan); (ii) 'harmonic' P_2 – 7.66 $\pm$ 0.14 − 9.54 $\pm$ 0.90 hours (marked

doi: https://doi.org/10.52526/25792776-23.70.1-23

in magenta); (iii) 'harmonic' P_3 – $5.69 \pm 0.08 - 6.37 \pm 0.10$ hours (marked in red); (iv) 'harmonic' P_4 – $4.45 \pm 0.19 - 4.88 \pm 0.23$ hours (marked in green); and (v) 'harmonic' P_5 – $3.66 \pm 0.03 - 3.88 \pm 0.05$ hours (marked in blue). All these periods are plotted in Fig. 1. The ratios of the average periods from each group of the same sequence as in Fig. 1 are shown in Fig. 2. For the calculation of the uncertainties found in the period ratios, we use the following relation:

$$\triangle \frac{P_i}{P_{i+1}} = \left| \frac{1}{P_{i+1}} \triangle P_i - \frac{P_i}{P_{i+1}^2} \triangle P_{i+1} \right| \leq \left| \frac{\triangle P_i}{P_{i+1}} \right| + \left| -\frac{P_i}{P_{i+1}^2} \triangle P_{i+1} \right|, \tag{2}$$

where $P_i > P_{i+1}$ ($i = 1, 2, \ldots$ is the number of 'harmonics' are the global and the total mean periods evaluated for each AR. They sequentially follow each other in descending order. The ratios of the averaged periods look like the sequence of oscillation harmonics typical for a standing oscillations. In Fig. 2 the reference values of the ratios are shown with black solid horizontal lines. We would like to point out that the observed ratios do not exactly coincide with the sequence of ratios of periods corresponding to the pure standing oscillations $(2/1, 3/2, 4/3, \ldots)$. However, we can say that these ratios with the entire uncertainty interval are well separated and approximately follow the reference spectrum ratios. Therefore, with the present level of accuracy the observed discrete spectrum follows the sequence of the quasi-standing oscillations with some shift of the periods and corresponding ratios from the reference values. The cause of this shift of the periods might be the incomplete line-tying of the magnetic loop system, or the Doppler shifts due to the internal flows in the ARs, and/or the inhomogeneity of the magnetic loop system constituting the AR below and above the solar surface.

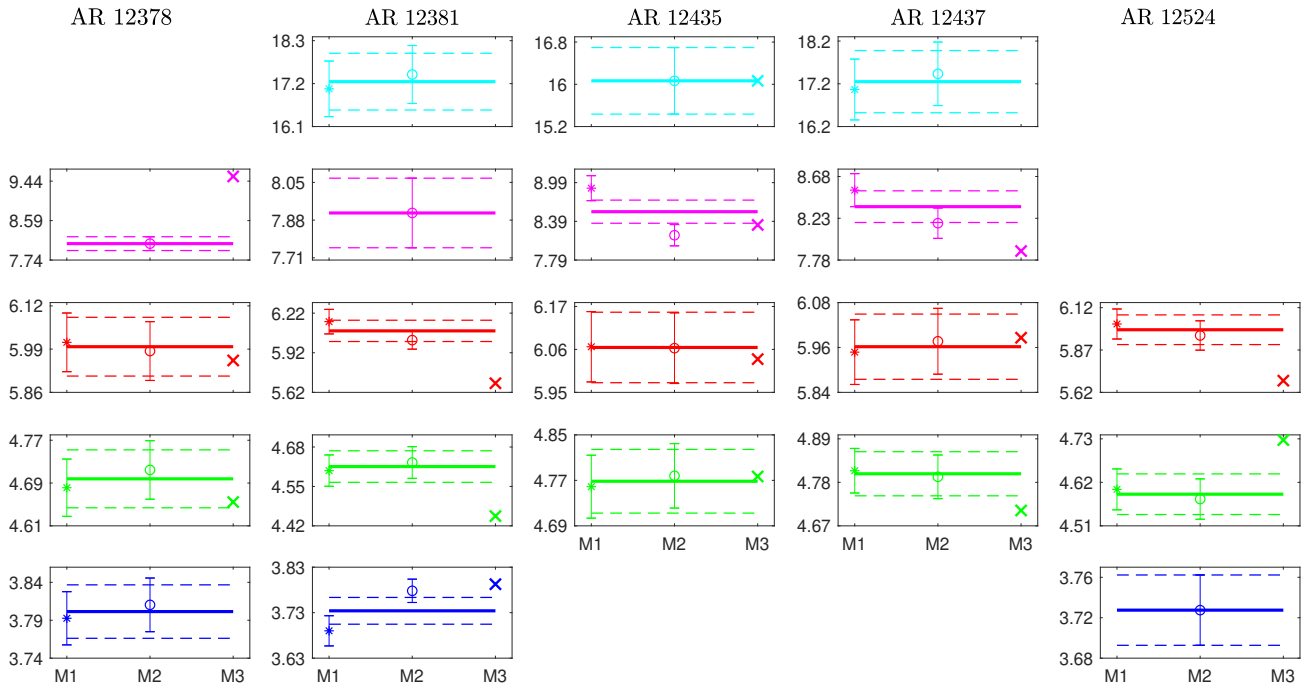

Figure 1. Characteristic mean oscillation periods (measured in hours) calculated as a global average of those found in different time series of the total area of the ARs and the total radial magnetic flux. On the horizontal axes, the M1, M2 and M3 labels, respectively, denote the global mean of the periods obtained by M1 (coloured '$*$' with error bars), M2 (coloured '$\circ$' with error bars), and M3 (coloured '$\times$' with error bars). Moreover, we also indicate the total mean periods by taking the average of the mentioned global means of M1 and M2 (*i.e.*, the mean periods obtained by M3 are excluded from the total mean calculation) via the solid-coloured horizontal lines (with the uncertainties indicated by the dashed coloured lines).

4. Conclusions

The next conclusions might be revealed:

- The most populated sets of the periods are obtained for the total area of the ARs;

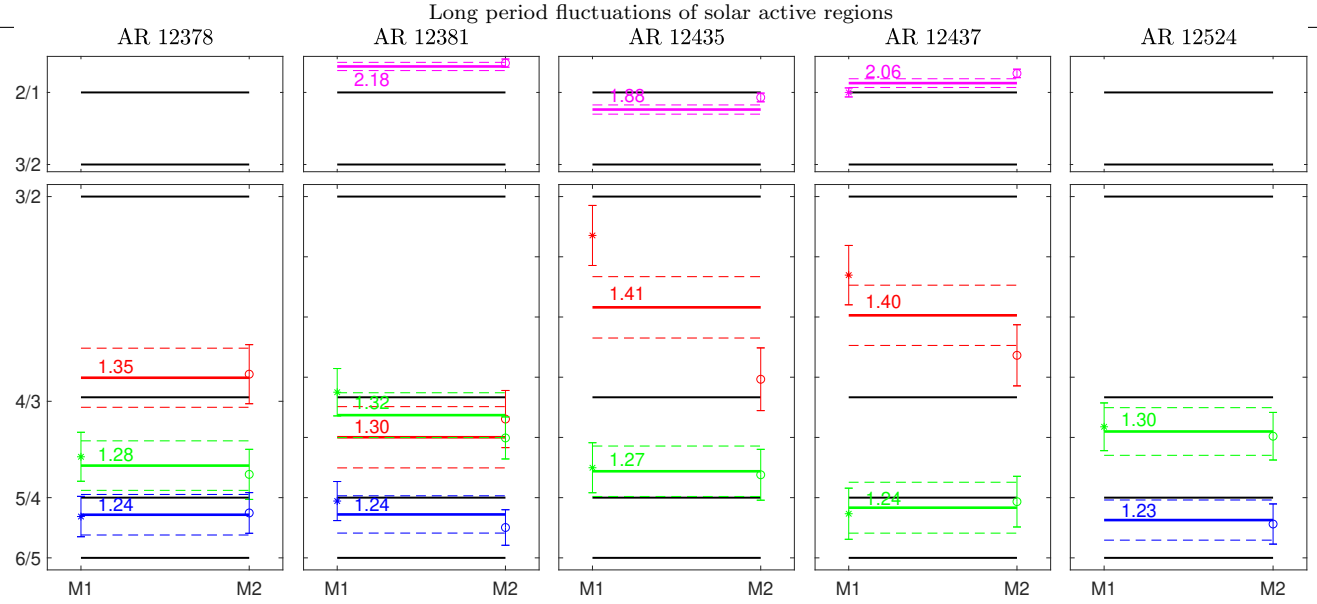

Figure 2. Ratios of global mean periods (P_i/P_{i+1}, $i = 1, 2, \ldots$) of M1, M2 and the total mean periods shown in the panels of Fig. 1. The formatting of the data points and horizontal lines is the same as in Fig. 1. The colouring in each panel coincides with the period standing in the denominator in each ratio. On the vertical axes, the levels of the period ratios in the reference spectrum are labelled and the corresponding horizontal solid black lines are plotted in all panels.

- In all analyzed datasets the long-period peaks that are > 10 hours can be detected less frequently than those of shorter periods < 10 hours;
- The radial unsigned magnetic flux data has some significant periods;
- In all datasets there are long-period oscillations with characteristic periods in the range from 2 to 20 hours;
- With the present level of accuracy the observed discrete spectrum follows the sequence of the quasi-standing oscillations with some shift of the periods and corresponding ratios from the reference values.

All of these long-period oscillation spectra need rigorous analytical or numerical modeling to understand their origin. The physical interpretation of the found oscillations requires the construction of rigorous mathematical models and this is beyond the scope of current purely observational study.

References

Appourchaux T., 2003, Astron. Astrophys. , 412, 903

Bobra M. G., Sun X., Hoeksema J. T., et al. 2014, Solar Physics, 289, 3549

Centeno R., Collados M., Trujillo Bueno J., 2006, Astrophys. J. , 640, 1153

Chorley N., Hnat B., Nakariakov V. M., et al. 2010, Astron. Astrophys. , 513, A27

Dumbadze G., Shergelashvili B. M., Kukhianidze V., et al. 2017, Astron. Astrophys. , 597, A93

Efremov V. I., Parfinenko L. D., Solov'ev A. A., 2007, Astronomy Reports, 51, 401

Gopasyuk O. S., 2004, in Multi-Wavelength Investigations of Solar Activity. pp 249–250

Khutsishvili E., Kvernadze T., Sikharulidze M., 1998, Solar Physics, 178, 271

Liu Y., Hoeksema J. T., Scherrer P. H., et al. 2012, Solar Physics, 279, 295

Press W. H., Teukolsky S. A., Vetterling W. T., et al. 2007, Numerical Recipes 3rd Edition: The Art of Scientific Computing. Cambridge University Press

Scherrer P. H., Schou J., Bush R. I., et al. 2012, Solar Physics, 275, 207

Shergelashvili B. M., Poedts S., 2005, Astron. Astrophys. , 438, 1083

Thomas J. H., Cram L. E., Nye A. H., 1984, Astrophys. J. , 285, 368